AIAA AVIATION Forum
June 15-19, 2020, VIRTUAL EVENT
AIAA AVIATION 2020 FORUM

10.2514/6.2020-2779

High Efficiency Tandem Propeller-CoFlow Jet Airfoil System in Cruise

Yan Ren * Yang Wang † Gecheng Zha ‡
Coral Gables, FL 33124
Dept. of Mechanical and Aerospace Engineering
University of Miami, Coral Gables, Florida 33124

Abstract

In this paper, the aerodynamic performance of 2D tandem propeller-CoFlow Jet (CFJ) active flow control airfoils in cruise flight is numerically studied. The tandem propeller-CFJ airfoil system is an integrated system with upstream and downstream CFJ airfoils, each has a propeller mounted above the airfoil suction surface.

The simulations employ 3D RANS solver with Spalart-Allmaras (S-A) turbulence model, 3rd order WENO scheme for the inviscid fluxes, and 2nd order central differencing for the viscous terms. The aerodynamic performance, energy expenditure, and flow field are compared between tandem wing systems with different downstream airfoil locations and angle of attack. The results show that the cruise efficiency is sensitive to the downstream airfoil angle of attack. Moreover, The wing-wing interaction effect on the aerodynamic performance is studied by comparing the optimum tandem propeller-CFJ airfoil system to the upstream airfoil and downstream airfoil only (without interaction) cases. It is observed that the wing-wing interaction increases the cruise efficiency significantly due to the energized flow of the propellers. The front propeller has a "pushing" effect accelerating the flow to the downstream airfoil. The downstream propeller has a "pulling" effect to accelerate the upstream flow. The downstream airfoil with higher angle of attack also induces an upwash and a higher circulation to the upstream airfoil. The optimal tandem airfoil interaction benefit observed in this paper appears to be attributed the proximity of the two airfoils, which are only one chord away horizontally with the rear airfoil 0.1 chord below the front one. This study may provide some guidance on the propeller interaction of a tandem wing. However, it does not include the important effect of the tip vortices and downwash of a 3D tandem wing system.

Nomenclature

CFJ	Co-flow jet
AoA	Angle of attack
LE	Leading Edge
TE	Trailing Edge
S	Planform area
c	Profile chord
U	Flow velocity
q	Dynamic pressure $0.5\,\rho\,U^2$
p	Static pressure
ρ	Air density

* Postdoc Researcher, Ph.D., AIAA member
† Graduate Student
‡ Professor, AIAA Associate Fellow, Professor of the University of Miami

$\dot{m}$	Mass flow
M	Mach number
P	Pumping power
∞	Free stream conditions
C_L	Lift coefficient $L/(q_\infty S)$
C_D	Drag coefficient $D/(q_\infty S)$
C_μ	Jet momentum coef. $\dot{m}_j U_j/(q_\infty S)$
P_c	CFJ power coefficient $L/(q_\infty S V_\infty)$
T_C	Propeller actuator thrust coefficient
P_{PC}	Propeller actuator power coefficient
C_T	Total thrust coefficient of the system
C_L/C_{PW}	Porpeller-CFJ airfoil corrected aerodynamic efficiency $C_L/(P_{PC}+P_c)$
C_L^2/C_{PW}	Porpeller-CFJ airfoil corrected productivity efficiency $C_L^2/(P_{PC}+P_c)$

1 Introduction

In nature, tandem wing configuration is widely adopted by insects, such as dragonflies and locusts. It is proven that such configuration could lead to superior stability and maneuverability, and could benefit the aerodynamic performance via active wing-wing interaction.

Tandem wing configuration has attracted a lot of interest recently due to the development of electric vertical takeoff/landing vehicles for urban air mobility[1, 2, 3]. The advantage of tandem wings is that it has high hovering stability due to two lifting vectors. However, it reduces the aircraft effective aspect ratio and the front wing's tip vortex and wake may affect the performance of the rear wing at cruise. How to optimize the tandem wing configuration to improve cruise efficiency is thus a very important topic, which is the purpose of this paper.

The rear wing of typical tandem wing aircraft usually locates above the front wing to avoid the wake of the upstream wing and the propeller, which is perceived to be harmful to the aerodynamic performance. However, with the help of the novel Co-Flow Jet (CFJ) flow control[4, 5, 6, 7, 8, 9, 10, 11, 12, 13, 14], the hind wing may benefit from the the incoming wake to improve the cruise efficiency.

In this work, we take a 2D tandem propeller-CFJ airfoil system as the model to study its performance at cruise without the downwash effect. The 2D tandem propeller-CFJ airfoil system studied is an integrated system with upstream and downstream CFJ airfoils, each has a propeller mounted above the wing suction surface as shown in Fig. 1. Parametric studies are conducted to investigate the effect of downstream airfoil vertical location and angle of attack with optimum cruise efficiency. The effect of the wing-wing interaction is studied by comparing the optimum tandem propeller-CFJ airfoil system to the upstream airfoil and downstream airfoil only (without interaction) cases. The results show that the wing-wing interaction can substantially increase the cruise efficiency. The conclusion of this work may provide some guidance for future 3D high-efficiency tandem propeller-CFJ aircraft design.

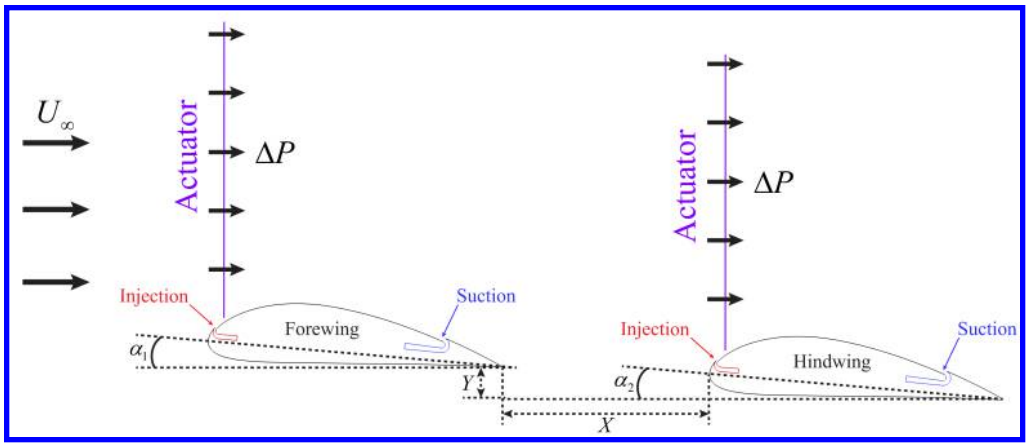

Figure 1: Schematic plot of a tandem propeller-CFJ airfoil system in the present study.

2 The Co-Flow Jet Airfoil

The CFJ airfoil has an injection slot near the leading edge(LE) and a suction slot near the trailing edge(TE) on the airfoil suction surface as sketched in Fig. 2. A small amount of mass flow is withdrawn into the airfoil near the TE, pressurized and energized by a micro-compressor system inside the airfoil, and then injected near the LE in the direction tangent to the main flow. The whole process does not add any mass flow to the system and hence is a zero-net mass-flux flow control.

The CFJ airfoil flow control mechanism achieves a radical lift augmentation, drag reduction and stall margin increase at a very low energy expenditure. It can not only achieve ultra-high maximum lift coefficient, but also significantly enhance cruise productivity efficiency and cruise wing loading from subsonic to transonic conditions[15, 16, 17, 18, 19, 20].

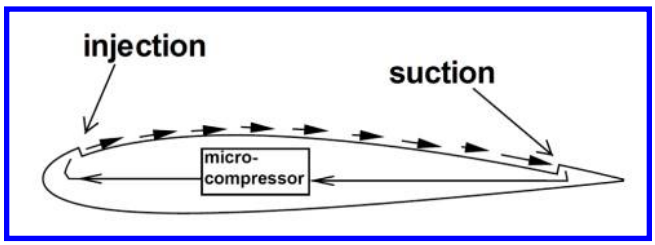

Figure 2: Baseline airfoil and CFJ Airfoil.

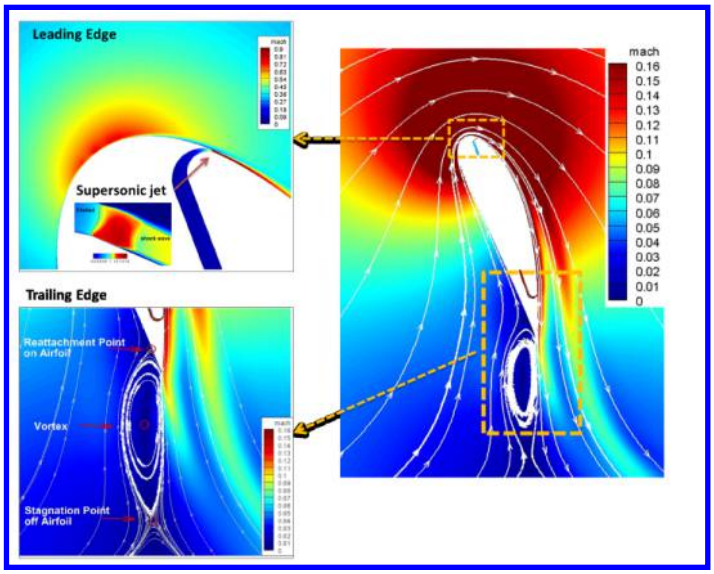

Figure 3: Mach number contours and streamlines at $C_\mu = 0.35$ and AoA =70° for the CFJ6421-SST016-SUC053-INJ009 airfoil.

Yang and Zha [19] discovered in 2017 that a CFJ airfoil can achieve Super-Lift Coefficient(SLC), which is a lift coefficient that exceeds the theoretical limit of potential flow developed by Smith[21] and is defined below:

$$C_{Lmax} = 2\pi(1 + \frac{t}{c}) \tag{1}$$

When a SLC occurs, the circulation is so high that the stagnation point is detached from the airfoil body as shown in Fig. 3, which has a C_{Lmax} of 10.6, far greater than the theoretical limit of 7.6. The freestream condition has a Mach number of 0.063 and Reynolds number of 3 million. The flow remains attached at AoA of 70° and the wake is filled with reversed velocity deficit, similar to the owl effect that generates very low wake turbulent noise. The CFJ airfoil pressure coefficient at the leading edge suction peak is nearly 10 times higher than the maximum value of the baseline airfoil at AoA of 18° before it stalls [19]. In other words, the CFJ airfoil at SLC condition can keep flow attached despite an adverse pressure gradient nearly one order of magnitude higher than the conventional airfoil. The simulation of Yang and Zha [19] also reveals a complex phenomenon with 4 layers of counter-rotating vortex layers emanating from leading edge and trailing to the wake of the airfoil. The detailed analysis can be seen in [19, 22].

3 CFJ Parameters

The following are the parameters used to define the propeller-CFJ airfoil performance.

3.1 Lift and Drag Calculation

The momentum and pressure at the injection and suction slots produce a reactionary force, which is automatically measured by the force balance in wind tunnel testing. However, for CFD simulation, the full reactionary force needs to be included. Using control volume analysis, the reactionary force can be calculated using the flow parameters at the injection and suction slot opening surfaces. Zha et al. [5] give the following formulations to calculate the lift and drag due to the jet reactionary force for a CFJ airfoil. By considering the effects of injection and suction jets on the CFJ airfoil, the expressions for these reactionary forces are given as :

$$F_{x_{cfj}} = (\dot{m}_j V_{j1} + p_{j1} A_{j1}) * cos(\theta_1 - \alpha) - (\dot{m}_j V_{j2} + p_{j2} A_{j2}) * cos(\theta_2 + \alpha) \tag{2}$$

$$F_{y_{cfj}} = (\dot{m}_{j1} V_{j1} + p_{j1} A_{j1}) * sin(\theta_1 - \alpha) + (\dot{m}_{j2} V_{j2} + p_{j2} A_{j2}) * sin(\theta_2 + \alpha) \tag{3}$$

where the subscripts 1 and 2 stand for the injection and suction respectively, and θ_1 and θ_2 are the angles between the injection and suction slot's surface and a line normal to the airfoil chord. α is the angle of attack.

The total lift and drag on the airfoil can then be expressed as:

$$D = R'_x - F_{x_{cfj}} \tag{4}$$

$$L = R'_y - F_{y_{cfj}} \tag{5}$$

where R'_x and R'_y are the surface integral of pressure and shear stress in x (drag) and y (lift) direction excluding the internal ducts of injection and suction. For CFJ wing simulations, the total lift and drag are calculated by integrating Eqs.(4) and (5) in the spanwise direction.

3.2 Jet Momentum Coefficient

The jet momentum coefficient C_μ is a parameter used to quantify the jet intensity. It is defined as:

$$C_\mu = \frac{\dot{m}V_j}{\frac{1}{2}\rho_\infty {V_\infty}^2 S} \tag{6}$$

where $\dot{m}$ is the injection mass flow, V_j is the mass-averaged injection velocity, ρ_∞ and V_∞ denote the free stream density and velocity, and S is the planform area.

3.3 Power Coefficient

CFJ is implemented by mounting a pumping system inside the wing that withdraws air from the suction slot and blows it into the injection slot. The power consumption is determined by the jet mass flow and total enthalpy change as the following:

$$P_{CFJ} = \dot{m}(H_{t1} - H_{t2}) \tag{7}$$

where H_{t1} and H_{t2} are the mass-averaged total enthalpy in the injection cavity and suction cavity respectively, P is the Power required by the pump and $\dot{m}$ the jet mass flow rate. Introducing P_{t1} and P_{t2} the mass-averaged total pressure in the injection and suction cavity respectively, the pump efficiency η, and the total pressure ratio of the pump $\Gamma = \frac{P_{t1}}{P_{t2}}$, the power consumption is expressed as:

$$P_{CFJ} = \frac{\dot{m}C_p T_{t2}}{\eta}(\Gamma^{\frac{\gamma-1}{\gamma}} - 1) \tag{8}$$

where γ is the specific heat ratio equal to 1.4 for air. The power coefficient for CFJ is expressed as:

$$P_c = \frac{P_{CFJ}}{\frac{1}{2}\rho_\infty V_\infty^3 S} \tag{9}$$

The power coefficient for the propeller actuator is:

$$P_{PC} = \frac{TV_\infty}{\frac{1}{2}\rho_\infty S V_\infty^3} = \frac{T}{\frac{1}{2}\rho_\infty S V_\infty^2} = T_C \tag{10}$$

where T is the propeller thrust force; T_C is the propeller thrust coefficient.

In order to compare the efficiency of a propeller-CFJ airfoil with that of a conventional airfoil, a corrected aerodynamic efficiency C_L/C_{PW} is introduced, which takes into consideration of the power needed for the CFJ[17] as well as the power needed for the propeller actuator:

$$\frac{C_L}{C_{PW}} = \frac{C_L}{P_C + P_{PC}} \tag{11}$$

where C_{PW} is the total power coefficient of the system, which has two components, the power coefficient of the CFJ, P_C, and the propeller actuator, P_{PC}. The C_L/C_{PW} incorporates the CFJ power consumption and the propeller power consumption. For a conventional airfoil with no CFJ, P_C=0 and $P_{PC} = C_D$, where C_D is the drag coefficient. In that case, CL/C_{PW} in Eq (11) returns to the conventional aerodynamic efficiency of C_L/C_D.

To measure aircraft transportation productivity defined by $Range \times Gross\ Weight$, a parameter C_L^2/C_D is introduced as the productivity efficiency[19]. The productivity efficiency is considered as a more comprehensive parameter than the conventional aerodynamic efficiency C_L/C_D to measure the merit of an airplane aerodynamic design for cruise performance. The former includes not only the information of C_L/C_D, but also the information of the aircraft weight represented by C_L.

For CFJ-propeller airfoil, the productivity efficiency should also include the CFJ power consumption and the propeller power consumption, and it is defined as below:

$$\frac{C_L^2}{C_{PW}} = \frac{C_L^2}{P_C + P_{PC}} \tag{12}$$

3.4 CFD Simulation Setup

The in house FASIP (Flow-Acoustics-Structure Interaction Package) CFD code is used to conduct the numerical simulation. The simulations employ 3D RANS solver with Spalart-Allmaras (S-A) turbulence model. A 3rd order WENO scheme for the inviscid flux [23, 24, 25, 26, 27, 28] and a 2nd order central differencing for the viscous terms [23, 27] are employed to discretize the Navier-Stokes equations. The low diffusion E-CUSP scheme used as the approximate Riemann solver suggested by Zha et al [24] is utilized with the WENO scheme to evaluate the inviscid fluxes. Implicit time marching method using Gauss-Seidel line relaxation is used to achieve a fast convergence rate [29]. Parallel computing is implemented to save wall clock simulation time [30].

3.5 Boundary Conditions

The 3rd order accuracy no slip condition is enforced on the solid surface with the wall treatment suggested in [31] to achieve the flux conservation on the wall. The computational mesh is shown in Fig. 4. Total pressure, total temperature and flow angles are specified at the injection duct inlet, as well as the upstream portion of the far field. Constant static pressure is applied at the suction duct outlet as well as the downstream portion of the far field. The total mesh size is 73,600 for all 2D cases, split into 48 blocks for the parallel computation. The domain boundary is about 300 chords away from the airfoil to ensure an accurate simulation. The first grid point on the wing surface is placed at $y^+ \approx 1$. The propeller is simulated using an actuator disk boundary condition with a pressure jump (ΔP) imposed. The pressure jump is given as a percentage of the pressure upstream of the actuator, typically is fairly small and rarely greater than 2%. The pressure jump condition can be very well handled by the Riemann solver employed in the FASIP CFD code. In this study, the ΔP for each propeller actuator disk is iterated to make the system resultant force in the flight direction to be zero for the cruise condition.

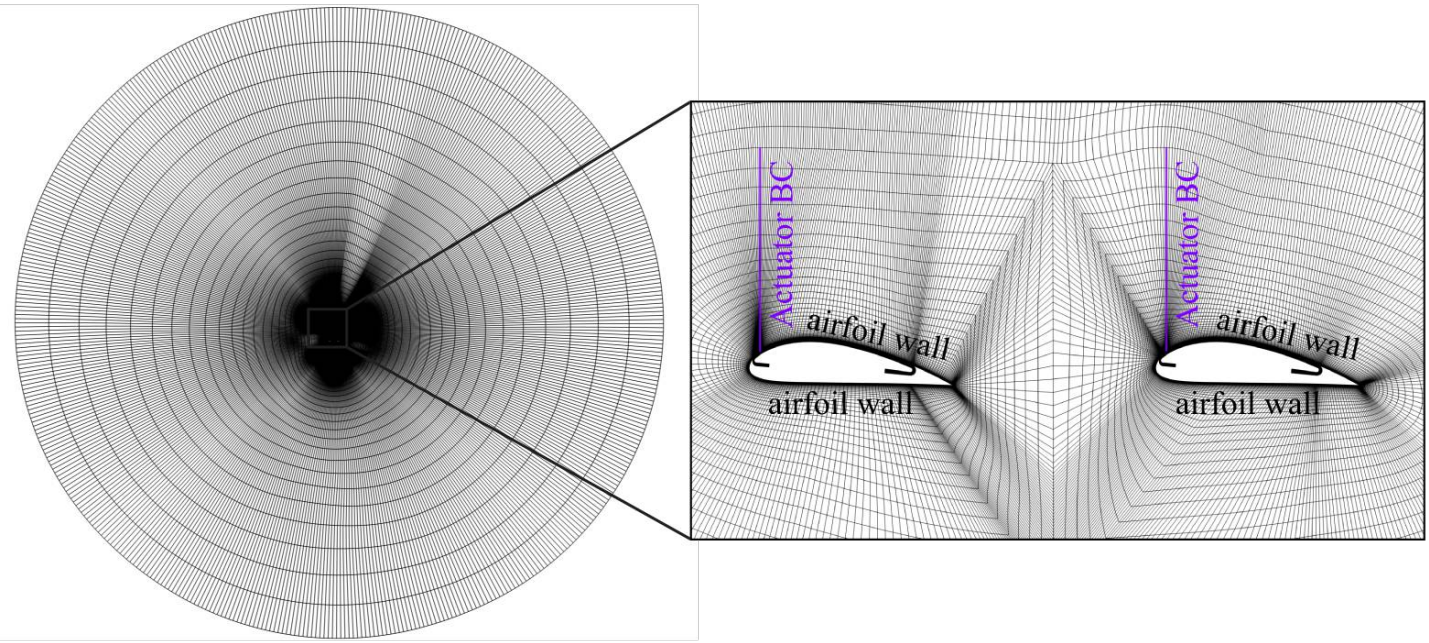

Figure 4: Computational mesh used in the current work.

4 Results and Discussion

The aerodynamic performance of tandem CFJ-propeller airfoils are investigated and presented in this section. The planform area $S = 1c$ for all 2D cases, which is convenient to compare the tandem airfoil system with the single airfoil cases. The momentum coefficient $C_\mu = 0.03$ is used for all the cases discussed here. The propeller strength is quantified by ΔP, which is iterated during the simulation to achieve an assumed total system thrust $C_T = 0.16$ for all tandem wing cases. The total system thrust is used to balance the hypothetical induced drag and the fuselage drag of the aircraft, which are not considered in these 2D simulations. Single wing cases are also disused in the present study. In order to perform a fair comparison between the tandem CFJ-propeller airfoil system and the single wing CFJ-propeller system, the C_T is configured as 0.08 (50% of the C_T used in tandem airfoil cases) for single wing cases.

The free stream Mach number for all cases are 0.15 and the propeller actuator disks are normal to the free stream. The propeller actuator is located near the airfoil leading edge, downstream of the injection slot and above the suction surface. This propeller position is optimized to interact with the CFJ airfoil to maximize the power efficiency for both VTOL hovering and cruise. All airfoils used in the current study are the CFJ-NACA-6421 optimized by Wang and Zha[32, 33, 34].

4.1 Effect of Downstream Airfoil Vertical Location and Angle of Attack

In this section, the aerodynamic effect of downstream airfoil vertical locations and angle of attack is discussed. As shown in Table 1, the upstream airfoil is held at angle of attack $\alpha_1 = 5°$, and the downstream airfoil has the AoA varying with $\alpha_2 = 5°, 7.5°, 10°, 12.5°$, and $15°$. The downstream airfoil horizontal location is fixed as $X = 1c$. The downstream airfoil vertical locations are $0.0c, -0.1c$, and $0.1c$ for cases A1-A5, B1-B5, and C1-C5, respectively.

Table 1: Simulation parameters used in the current work.

Cases	X	Y	α_1	α_2	M_∞	C_μ	C_T
A1	1c	0.0c	5°	5°	0.15	0.03	0.16
A2				7.5°			
A3				10°			
A4				12.5°			
A5				15°			
B1	1c	-0.1c	5°	5°	0.15	0.03	0.16
B2				7.5°			
B3				10°			
B4				12.5°			
B5				15°			
C1	1c	0.1c	5°	5°	0.15	0.03	0.16
C2				7.5°			
C3				10°			
C4				12.5°			
C5				15°			

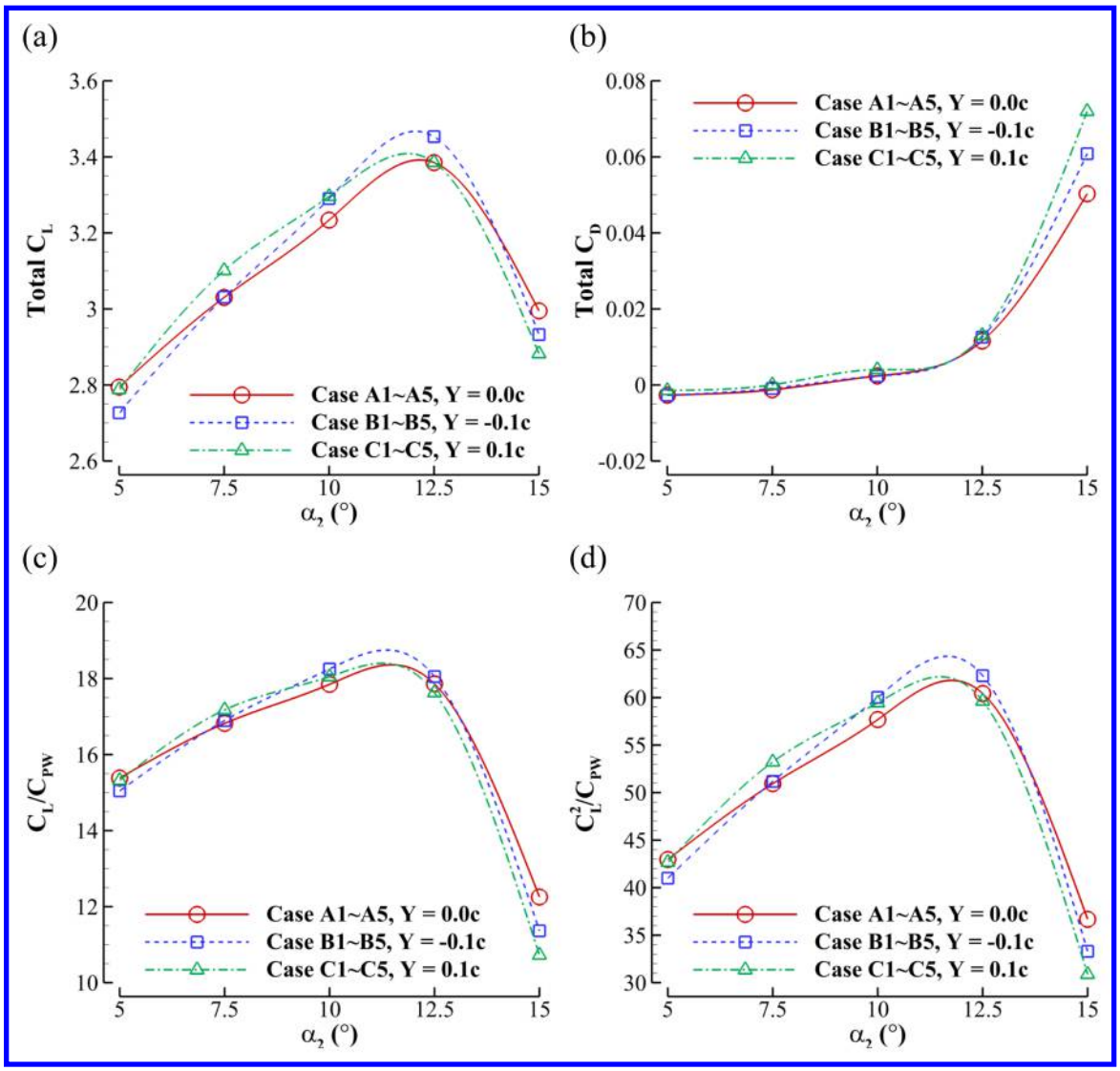

Figure 5: Aerodynamic performance of the tandem propeller-CFJ airfoils in cruise; (a) total C_L, (b) total C_D, (c) C_L/C_{PW}, and (d) C_L^2/C_{PW}.

Fig. 5 shows the total C_L, C_D, C_L/C_{PW}, and C_L^2/C_{PW} for all cases. We can see that the aerodynamic performance is more sensitive to the downstream airfoil angle of attack α_2 than the vertical location Y. However, a lower position of the downstream airfoil shows a better efficiency because its suction surface receives more energized flow from the upstream propeller wake. Case B4 has the highest lift coefficient and productivity efficiency. Case B3 has the best aerodynamic efficiency and relatively high lift production. Compared with Case A1, the aerodynamic efficiency of case B3 is increased about 18.7%, and the productivity efficiency of case B4 is increased about 49.7%.

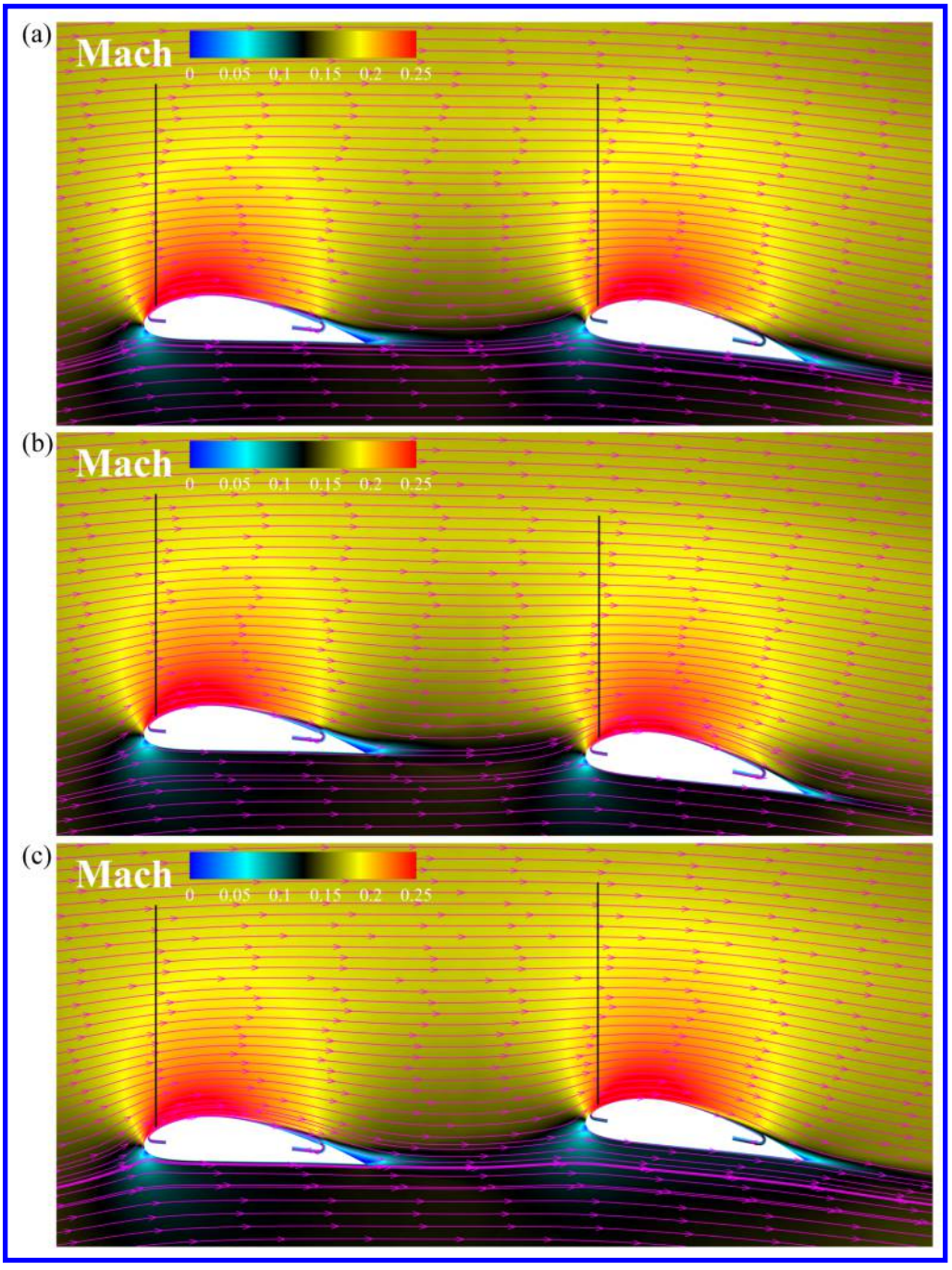

Figure 6: Mach contours and streamlines of (a) case A3, (b) case B3, and (c) case C3.

Fig. 6 shows the Mach contours and streamlines of case A3, B3, and C3. All three cases have fairly high aerodynamic efficiency. A very small separation can be seen at the trailing edge of the upstream airfoil for all cases. The upstream airfoil propeller wake approaches the leading edge of the downstream airfoil and is turned by the CFJ airfoil. The flow turning at the downstream airfoil of case C3 is larger than the front airfoil due to its position above the front airfoil, but the flow separation at the trailing edge is smaller and is benefited from the energized propeller wake flow.

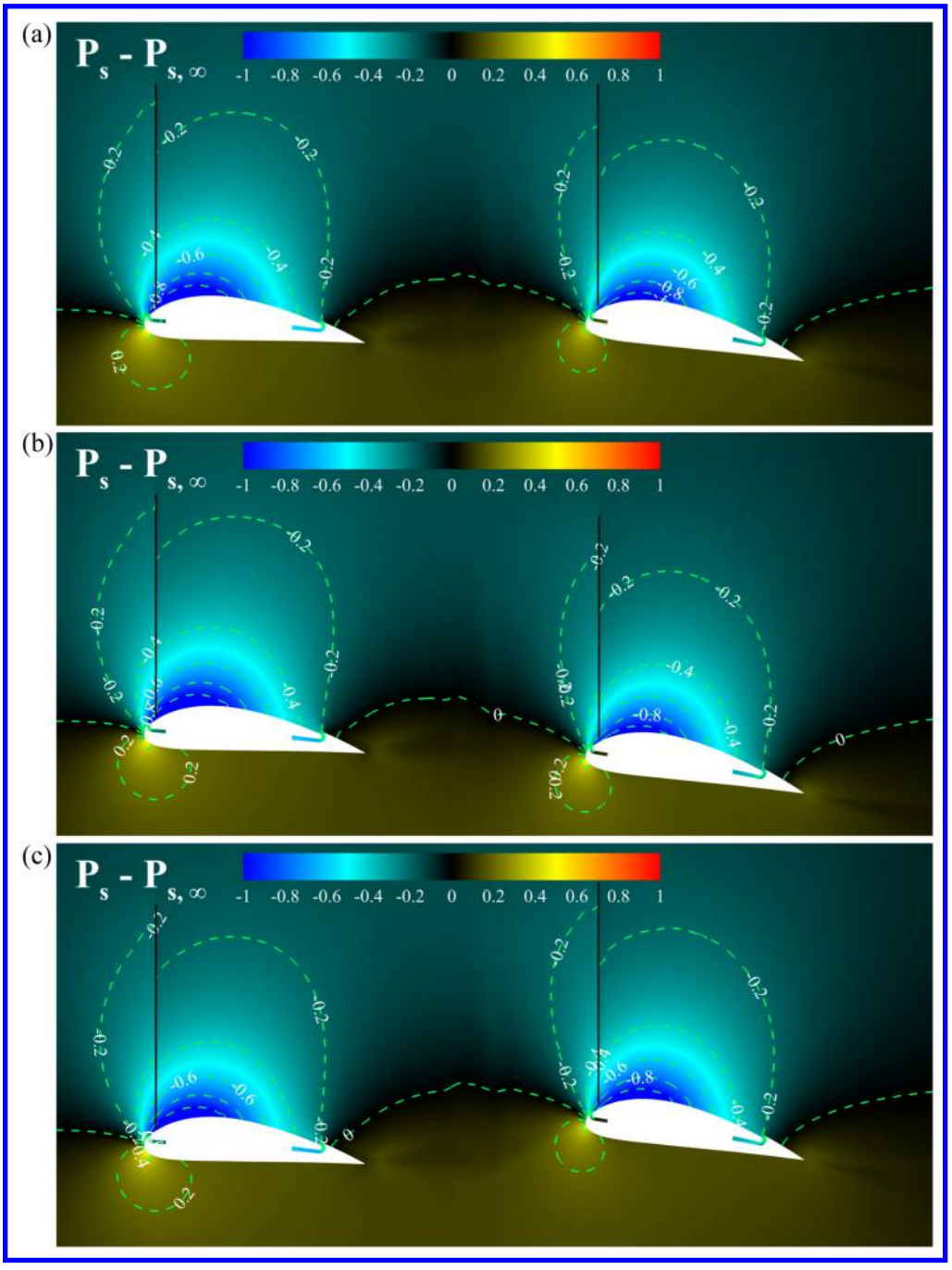

Figure 7: C_P contours of (a) case A3, (b) case B3, and (c) case C3.

Fig. 7 shows the C_P contours of the three cases. The propeller actuator disk creates a static pressure discontinuity that can be observed in Fig. 7. The C_P contours looks similar for all cases. The downstream airfoil of case C3 shows a larger low pressure region above the suction surface due to a larger flow turning.

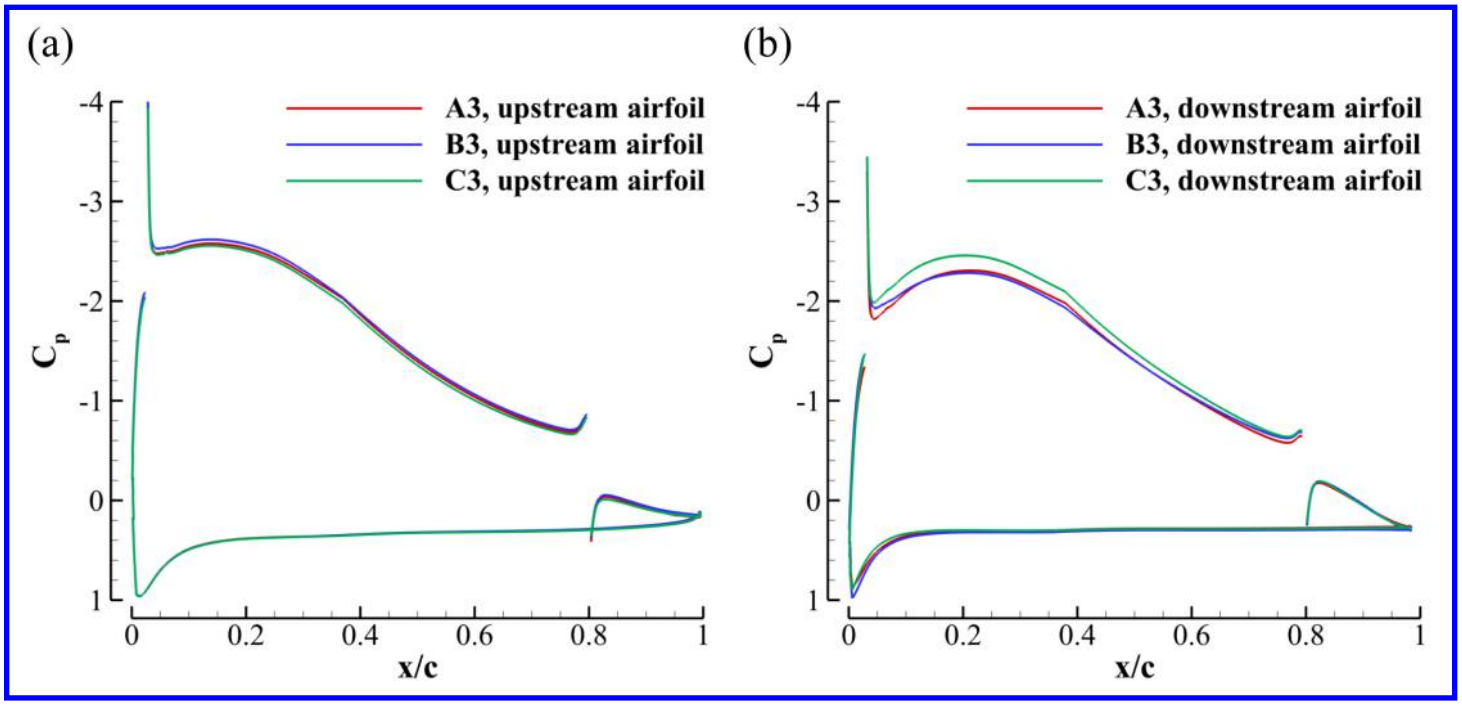

Figure 8: C_P distributions on the airfoil surface; (a) upstream airfoil of case A3, B3, and C3, (b) downstream airfoil of case A3, B3, and C3.

Fig. 8 shows the pressure coefficient distributions on the upstream airfoil and downstream airfoil of the tandem propeller-CFJ system. The discontinuity of the curves are due to the injection and suction slots of the CFJ airfoils. From Fig. 8, we can see that the C_p distribution on the pressure surfaces are almost the same for all cases. The case B3 has lower C_p distribution on the upstream airfoil suction surface. For the hind wing suction surface, case C3 shows a clearly lower C_p distribution on the suction surface, which leads to a higher lift and drag production for the downstream airfoil.

In summary, the downstream airfoil angle of attack α_2 has a large effect on the tandem wing system aerodynamic performance. The optimum α_2 is 10° for the aerodynamic efficiency and is 12.5° for the productivity efficiency. The optimum downstream airfoil vertical location Y is -0.1c for both aerodynamic and productivity efficiencies.

4.2 Effect of Wing-Wing Interaction

In this section, the effect of wing-wing interaction is investigated by comparing the optimum aerodynamic efficiency case B3 to two single wing cases S1 and S2. The case parameters and results are listed in Table 2. The airfoil in case S1 has the same angle of attack as the upstream airfoil of case B3, and the airfoil in case S2 has the same angle of attack as the downstream airfoil of case B3. The flow conditions and CFJ configuartions of the single wing cases are the same as case B3.

As shown in Table 2, the lift production of both wings of case B3 show much greater C_L comparing to the single

wing cases. The lift augmentation is 23.6% for the upstream airfoil and is 10.24% for the downstream airfoil. The total 2D profile drag of case B3 decreases 94.5% comparing to that of the single wing cases, which leads to the propeller power coefficient P_{PC} reduces by 17.35%. In addition, the CFJ power coefficient P_C also decreases for both upstream and downstream airfoils by 18.08% and 65.61%, respectively. The aerodynamic efficiency of case B3 is increased by 59.8% and the productivity efficiency is almost doubled (96.9%).

Table 2: Case parameters and aerodynamic performance of case B3 and single wing cases S1 and S2.

Case	Airfoils	α	M_∞	C_μ	C_T	C_L	C_D	P_c	P_{PC}	C_L/C_{PW}	C_L^2/C_{PW}
B3	Upstream	5°	0.15	0.03	0.16	1.73	-0.102	0.00852	0.162	18.25	60.02
	Downstream	10°				1.56	0.104	0.00932			
S1	Single wing	5°			0.08	1.40	-0.00458	0.0104	0.196	11.42	30.48
S2	Single wing	10°			0.08	1.27	0.0407	0.0271			

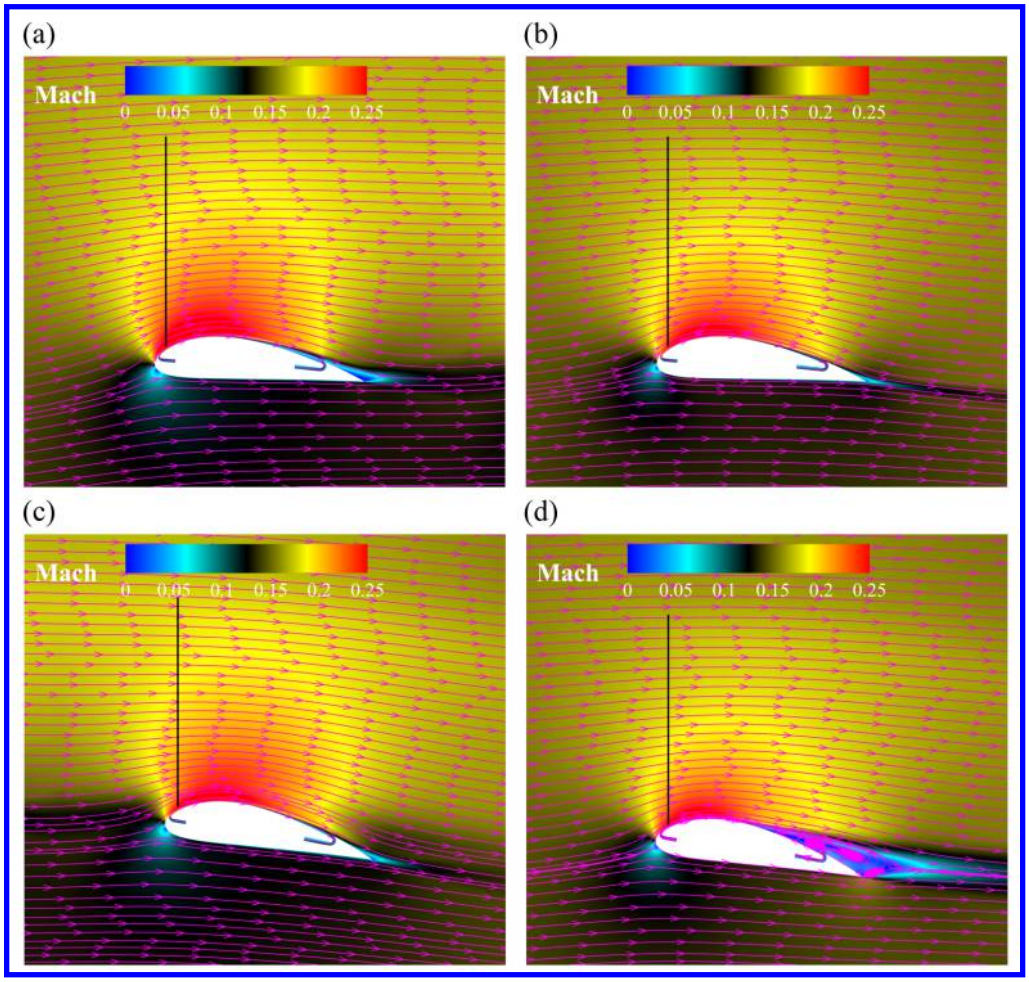

Figure 9: Mach contours and streamlines of (a) upstream airfoil of case B3, (b) upstream single airfoil only case S1, (c) downstream airfoil of case B3, and (d) downstream single airfoil only case S2.

Fig. 9 shows the Mach contours and streamlines of case B3 and the two single wing cases. As shown in Fig. 9 (a) and (b), the high velocity region above the suction surface of the upstream airfoil of case B3 is larger than the

single upstream airfoil only case. This effect appears to be benefited from the "pulling" effect of the downstream propeller, which accelerates the flow of the upstream airfoil. Due to a higher lift loading, the upstream airfoil shows a slightly larger low momentum region at the trailing edge than the single airfoil since they both have the same CFJ momentum coefficient of 0.03 and AoA. For the downstream airfoil, large separation can be observed near the trailing edge of the downstream single airfoil only case (Fig. 9 d) since the airfoil is at a high AoA of 10°. However, the flow is nicely attached to the downstream airfoil surface of the tandem wing system case B3. This appears to be benefited by the "pushing" effect of the upstream propeller that accelerates and energizes the flow to the downstream airfoil. In other words, the propellers may help each other in a tandem wing system if they are positioned properly. For the Case B3, the two wings are only one chord apart in the streamwise direction and 0.1 Chord apart vertically. This may have similar effect of dragonfly's tandem wing, but is overall a very close distance for an aircraft tandem wing system. Its feasibility for aircraft needs to be further studied, in particular for 3D wing with tip vortices effect.

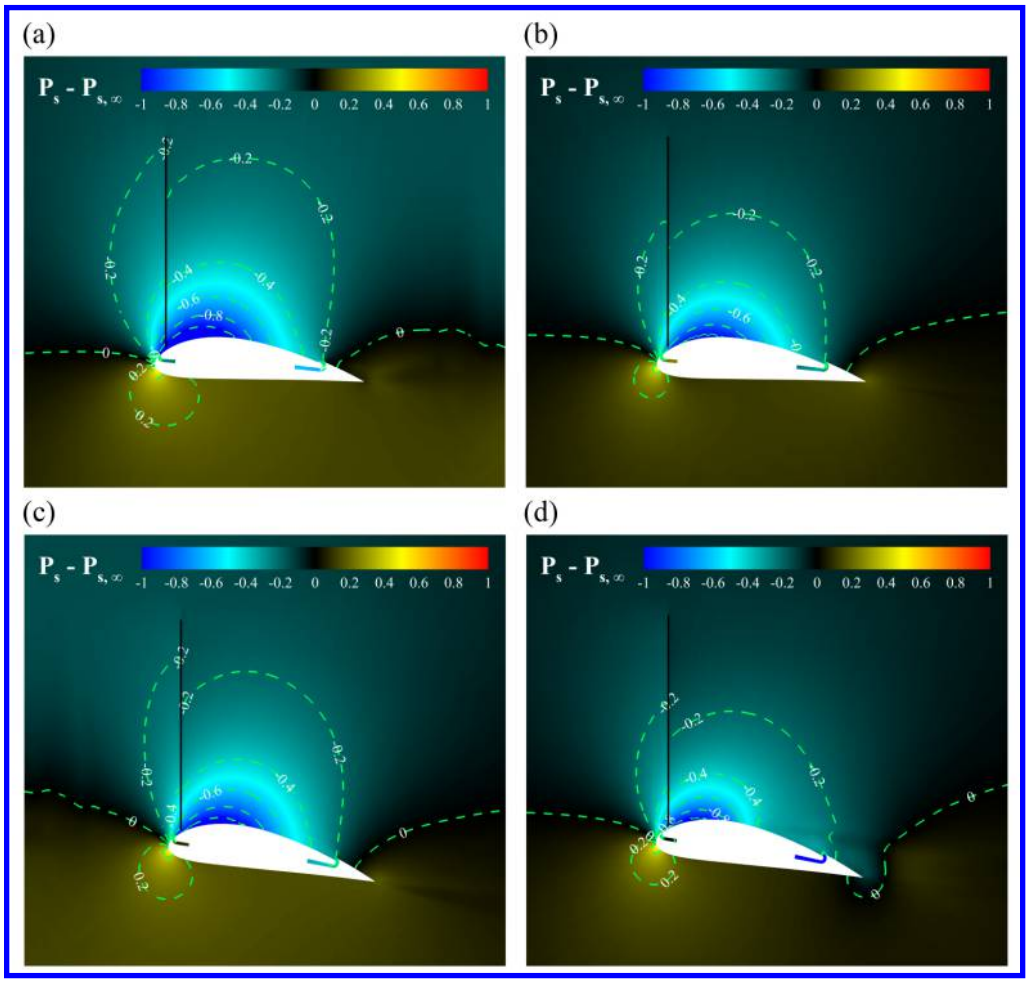

Figure 10: C_P contours of (a) upstream airfoil of case B3, (b) upstream single airfoil only case S1, (c) downstream airfoil of case B3, and (d) downstream single airfoil only case S2.

Fig. 10 shows the C_P contours of the case B3 and single wing cases. Both the upstream and downstream airfoil of case B3 show a larger low pressure region above the suction surfaces comparing to the upstream and downstream single airfoil only cases.

The pressure coefficient distributions on the propeller-CFJ airfoil surfaces for case B3 and single wing cases are shown in Fig. 11. For the front airfoil, the suction surface C_P is lower for both upstream and downstream airfoils of case B3, while the pressure surface C_P is larger. It leads to a greater surface pressure difference for the tandem propeller-CFJ system with a higher lift coefficient. The Cp distribution of the front wing in Fig. 11 indicates that the airfoil experiences a higher actual AoA than the single airfoil case even though they both are positioned with the same angle of attack of 5°. It thus has more circulation and higher lift. This effect can be attributed to the downstream airfoil positioned at a high AoA of 10° that generates some upwash effect to the airfoil one chord upstream.

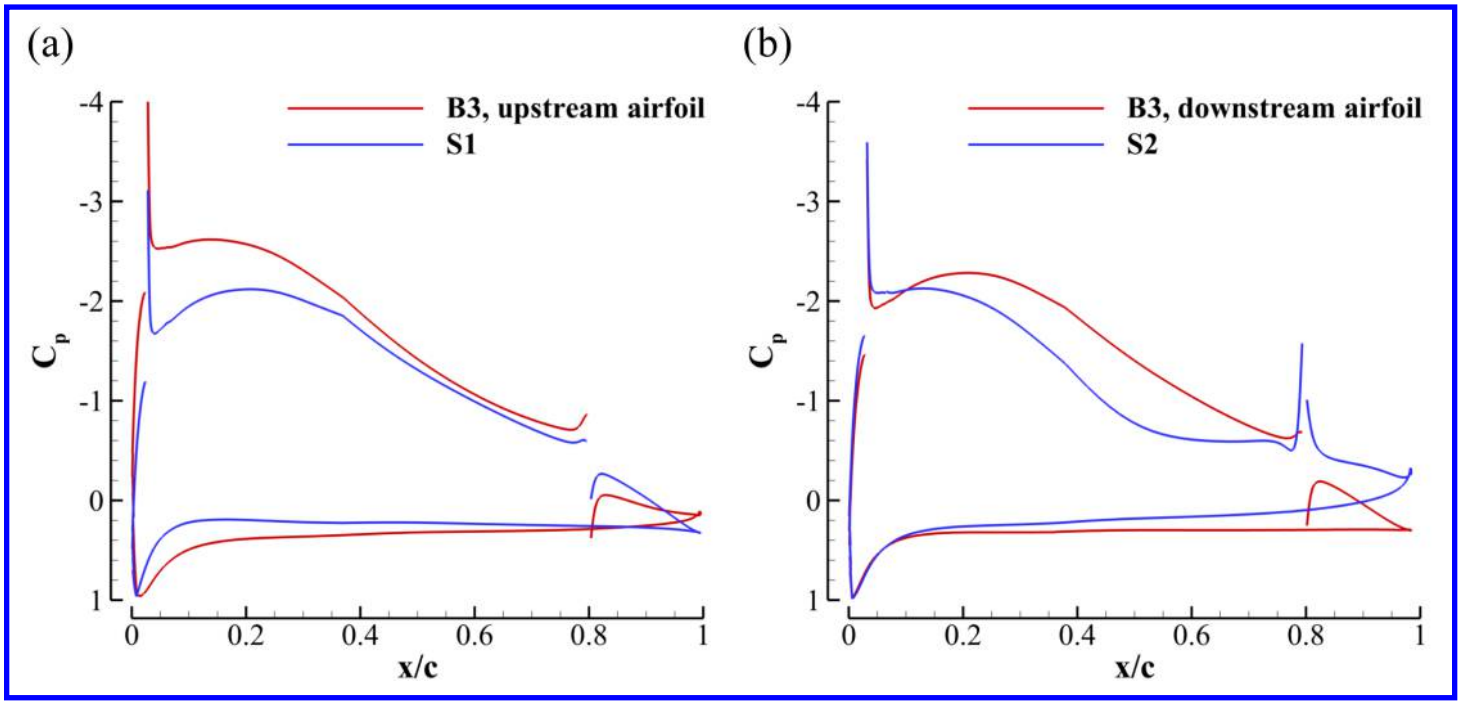

Figure 11: C_P distributions on the airfoil surface of case B3 and single wing cases S1 and S2.

5 Conclusion

The aerodynamic performance of a tandem propeller-CFJ airfoil system is numerically studied in cruise condiction. The results show that the downstream airfoil angle of attack α_2 has significant effect on the system aerodynamic performance. The optimal tandem airfoil interaction benefit observed in this paper appears to be attributed the proximity of the two airfoils, which are only one chord away horizontally with the rear airfoil 0.1 chord below the front one. The optimum α_2 is 10° for aerodynamic efficiency and is 12.5° for productivity efficiency. Compared with the single airfoil, the wing-wing interaction shows a benefit in the tandem propeller-CFJ airfoil system due to the energized flow by the propellers. The front propeller has a "pushing" effect accelerating the flow to the downstream airfoil. The downstream propeller has a "pulling" effect to accelerate the upstream flow. The downstream airfoil with higher angle of attack also induces an upwash and a higher circulation to the upstream airfoil. This study may provide some guidance on the propeller interaction of a tandem wing system. However, it does not include the important effect of the tip vortices and downwash of a 3D tandem wing system. The interaction effect with a farther distance between the two wings also need to be studied.

6 Acknowledgment

We are very grateful to Emil Buehler Perpetual Trust for their support for our research on green aviation at the University of Miami.

Disclosure: The University of Miami and Dr. Gecheng Zha may receive royalties for future commercialization of the intellectual property used in this study.

References

[1] Uber Elevate, "Fast-Forwarding to a Future of On-Demand Urban Air Transportation." Uber White Paper, Oct. 27, 2016.

[2] G.-C. Zha, Y. Ren, J.-Y. Gan, and D. Espinal, "A High Efficiency Low Noise VTOL/ESTOL Concept Using CoFLow Jet Airfoil." AIAA Paper 2019-4467, AIAA Propulsion and Energy 2019 Forum, Indianapolis, Indiana, 19-22 August 2019.

[3] J. Boling, G.-C. Zha, and C. Zeune, " High Speed High Efficiency VTOL Aircraft Using CoFlow Jet Active Flow Control Wings." Proceedings of 2020 AIAA Aviation Forum, Reno, Nevada, 15-19 June, 2020.

[4] G.-C. Zha and D. C. Paxton, "A Novel Flow Control Method for Airfoil Performance Enhancement Using Co-Flow Jet." *Applications of Circulation Control Technologies*, Chapter 10, p. 293-314, Vol. 214, Progress in Astronautics and Aeronautics, AIAA Book Series, Editors: Joslin, R. D. and Jones, G.S., 2006.

[5] G.-C. Zha, W. Gao, and C. Paxton, "Jet Effects on Co-Flow Jet Airfoil Performance," *AIAA Journal, No. 6,*, vol. 45, pp. 1222–1231, 2007.

[6] G.-C. Zha, C. Paxton, A. Conley, A. Wells, and B. Carroll, "Effect of Injection Slot Size on High Performance Co-Flow Jet Airfoil," *AIAA Journal of Aircraft*, vol. 43, 2006.

[7] G.-C. Zha, B. Carroll, C. Paxton, A. Conley, and A. Wells, "High Performance Airfoil with Co-Flow Jet Flow Control," *AIAA Journal*, vol. 45, 2007.

[8] Wang, B.-Y. and Haddoukessouni, B. and Levy, J. and Zha, G.-C., "Numerical Investigations of Injection Slot Size Effect on the Performance of Co-Flow Jet Airfoil," *Journal of Aircraft*, vol. Vol. 45, No. 6,, pp. pp.2084–2091, 2008.

[9] B. P. E. Dano, D. Kirk, and G.-C. Zha, "Experimental Investigation of Jet Mixing Mechanism of Co- Flow Jet Airfoil." AIAA-2010-4421, 5th AIAA Flow Control Conference, Chicago, IL, 28 Jun - 1 Jul 2010.

[10] B. P. E. Dano, G.-C. Zha, and M. Castillo, "Experimental Study of Co-Flow Jet Airfoil Performance Enhancement Using Micro Discreet Jets." AIAA Paper 2011-0941, 49th AIAA Aerospace Sciences Meeting, Orlando, FL, 4-7 January 2011.

[11] A. Lefebvre, B. Dano, W. Bartow, M. Fronzo, and G. Zha, "Performance and energy expenditure of coflow jet airfoil with variation of mach number," *Journal of Aircraft*, vol. 53, no. 6, pp. 1757–1767, 2016.

[12] A. Lefebvre, G-C. Zha, "Numerical Simulation of Pitching Airfoil Performance Enhancement Using Co-Flow Jet Flow Control," *AIAA paper 2013-2517*, June 2013.

[13] A. Lefebvre, G-C. Zha, "Cow-Flow Jet Airfoil Trade Study Part I : Energy Consumption and Aerodynamic Performance," *32nd AIAA Applied Aerodynamics Conference, AIAA AVIATION Forum, AIAA 2014-2682*, June 2014.

[14] A. Lefebvre, G-C. Zha, "Cow-Flow Jet Airfoil Trade Study Part II : Moment and Drag," *32nd AIAA Applied Aerodynamics Conference, AIAA AVIATION Forum, AIAA 2014-2683*, June 2014.

[15] Lefebvre, A. and Zha, G.-C. , "Design of High Wing Loading Compact Electric Airplane Utilizing Co-Flow Jet Flow Control." AIAA Paper 2015-0772, AIAA SciTech2015: 53nd Aerospace Sciences Meeting, Kissimmee, FL, 5-9 Jan 2015.

[16] Lefebvre, A. and Zha, G.-C., "Trade Study of 3D Co-Flow Jet Wing for Cruise and Takeoff/Landing Performance." AIAA Paper 2016-0570, AIAA SCITECH2016, AIAA Aerospace Science Meeting, San Diego, CA, 4-8 January 2016.

[17] Lefebvre, A. and Dano, B. and Bartow, W. and Di Franzo, M. and Zha, G.-C., "Performance Enhancement and Energy Expenditure of Co-Flow Jet Airfoil with Variation of Mach Number." AIAA Paper 2013-0490, AIAA Journal of Aircraft, DOI: 10.2514/1.C033113, 2016.

[18] Liu, Z.-X. and Zha, G.-C., "Transonic Airfoil Performance Enhancement Using Co-Flow Jet Active Flow Control." AIAA Paper 2016-3472, AIAA AVIATION 2016, 8th AIAA Flow Control Conference, Washington, D.C, June 13-17, 2016.

[19] Yang, Y.-C. and Zha, G.-C., "Super-Lift Coefficient of Active Flow Control Airfoil: What Is the Limit?." AIAA Paper 2017-1693, AIAA SCITECH2017, 55th AIAA Aerospace Science Meeting, Grapevine, Texas, 9-13 January 2017.

[20] G.-C. Zha, Y.-C. Yang, Y. Ren, and B. McBreen, "Super-lift and thrusting airfoil of coflow jet-actuated by micro-compressors." AIAA Paper 2017-3061, AIAA AVIATION 2018, Atlanta, GA , 25 - 29 June 2018.

[21] A. Smith, "High-Lift Aerodynamics," *Journal of Aircraft*, vol. 12, pp. 501–530, 1975.

[22] G.-C. Zha, "Estol performance for heavy lift transports using ultra-high lift high efficiency co-flow jet airfoil." Final Report to DARPA for Contract HR0011-16-2-0052, May 25, 2018.

[23] Y.-Q. Shen and G.-C. Zha, "Large Eddy Simulation Using a New Set of Sixth Order Schemes for Compressible Viscous Terms ," *Journal of Computational Physics*, vol. 229, pp. 8296–8312, 2010.

[24] Zha, G.C., Shen, Y.Q. and Wang, B.Y., "An improved low diffusion E-CUSP upwind scheme ," *Journal of Computer and Fluids*, vol. 48, pp. 214–220, Sep. 2011.

[25] Y.-Q. Shen and G.-Z. Zha , "Generalized finite compact difference scheme for shock/complex flowfield interaction," *Journal of Computational Physics*, vol. doi:10.1016/j.jcp.2011.01.039, 2011.

[26] Shen, Y.-Q. and Zha, G.-C. and Wang, B.-Y., " Improvement of Stability and Accuracy of Implicit WENO Scheme," *AIAA Journal*, vol. 47, No. 2, pp. 331–344, 2009.

[27] Shen, Y.-Q. and Zha, G.-C. and Chen, X.-Y., " High Order Conservative Differencing for Viscous Terms and the Application to Vortex-Induced Vibration Flows," *Journal of Computational Physics*, vol. 228(2), pp. 8283–8300, 2009.

[28] Shen, Y.-Q. and Zha, G.-C. , " Improvement of the WENO Scheme Smoothness Estimator," *International Journal for Numerical Methods in Fluids*, vol. DOI:10.1002/fld.2186, 2009.

[29] G.-C. Zha and E. Bilgen, "Numerical Study of Three-Dimensional Transonic Flows Using Unfactored Upwind-Relaxation Sweeping Algorithm," *Journal of Computational Physics*, vol. 125, pp. 425–433, 1996.

[30] B.-Y. Wang and G.-C. Zha, "A General Sub-Domain Boundary Mapping Procedure For Structured Grid CFD Parallel Computation," *AIAA Journal of Aerospace Computing, Information, and Communication*, vol. 5, No.11, pp. 2084–2091, 2008.

[31] Y.-Q. Shen, G.-C. Zha, and B.-Y. Wang, "Improvement of Stability and Accuracy of Implicit WENO Scheme ," *AIAA Journal*, vol. 47, pp. 331–344, 2009.

[32] Y. Wang and G.-C. Zha, "Study of 3D Co-flow Jet Wing Induced Drag and Power Consumption at Cruise Conditions." AIAA Paper 2019-0034, AIAA SciTech 2019, San Diego, CA, January 7-11, 2019.

[33] Y. Wang, Y.-C. Yang, and G.-C. Zha, "Study of Super-Lift Coefficient of Co-Flow Jet Airfoil and Its Power Consumption." AIAA Paper 2019-3652, AIAA Aviation 2019, AIAA Applied Aerodynamics Conference, Dallas, Texas, 17-21 June 2019.

[34] Y. Wang and G.-C. Zha, "Study of Mach Number Effect for 2D Co-Flow Jet Airfoil at Cruise Conditions." AIAA Paper 2019-3169, AIAA Aviation 2019, AIAA Applied Aerodynamics Conference, Dallas, Texas, 17-21 June 2019.